Eur. Phys. J. A (2017) **53**: 24
DOI 10.1140/epja/i2017-12215-8

THE EUROPEAN PHYSICAL JOURNAL A

Regular Article – Experimental Physics

In-beam study of ^{253}No using the SAGE spectrometer

A.K. Mistry[1,a], R.-D. Herzberg[1], P.T. Greenlees[2], P. Papadakis[2], K. Auranen[2,b], P.A. Butler[1], D.M. Cox[1,c], A.B. Garnsworthy[3], T. Grahn[2], K. Hauschild[4], U. Jakobsson[2], D.T. Joss[1], R. Julin[2], S. Ketelhut[3], J. Konki[2], M. Leino[2], A. Lopez-Martens[4], R.D. Page[1], J. Pakarinen[2], P. Peura[2], P. Rahkila[2], M. Sandzelius[2], C. Scholey[2], J. Simpson[5], D. Seddon[1], J. Sorri[2], S. Stolze[2], J. Thornhill[1], J. Uusitalo[2], and D. Wells[1]

[1] Oliver Lodge Laboratory, University of Liverpool, Liverpool, L69 7ZE, UK
[2] University of Jyvaskyla, Department of Physics, P.O. Box 35, FI-40014 Jyvaskyla, Finland
[3] TRIUMF, University of British Columbia, Vancouver, British Columbia V6T 2A3, Canada
[4] CSNSM, CNRS, IN2P3, Université Paris-Sud, F-91405 Orsay, France
[5] STFC, Daresbury Laboratory, Daresbury, Warrington, WA4 4AD, UK

Received: 17 October 2016 / Revised: 13 January 2017
Published online: 14 February 2017

Communicated by N. Kalantar

Abstract. The heavy actinide nucleus ^{253}No ($Z = 102$) was studied using the (S)ilicon (A)nd (Ge)rmanium (SAGE) spectrometer allowing simultaneous in-beam γ-ray and conversion electron spectroscopy at the accelerator laboratory of the University of Jyväskylä. Using the recoil-tagging technique, γ-electron coincidences have allowed for the extension of the level scheme in the lower-spin region of the yrast band. In addition, internal conversion coefficient (ICC) measurements to establish the multipolarity of transitions have been performed. Measurement of the interband-intraband branching ratios supports the assignment of the Nilsson band-head configuration $9/2^-[734]$ assigned in previous studies. The study shows the viability of combined in-beam electron and γ-ray spectroscopy down to μb cross sections.

1 Introduction

In-beam studies in the heavy element region around $Z \sim 102$ have proven fruitful, as they probe the single-particle orbitals originating from spherical nuclei around $Z = 120$. These orbitals slope down in energy with increasing deformation to lie close to the Fermi surface in this deformed mid-shell region. Such studies benefit from the relatively large production cross sections in fusion reactions with doubly magic ^{48}Ca on targets around ^{208}Pb. In recent years advances in experimental sensitivity have allowed in-beam spectroscopic studies of nuclei produced at sub-μb levels. One of the drivers of these developments was the study of the heaviest actinide and transactinide nuclei [1,2]. Indeed in-beam studies using gamma-ray spectroscopy of ^{256}Rf have been possible on cross sections as low as 17 nb [3].

Information on the ground-state configuration of ^{253}No is available from decay spectroscopy studies following the separation of evaporation residues [4–6] with the Nilsson single-neutron assignment ($\Omega^\pi[Nn_z\lambda]$) of $9/2^-[734]$ established. A number of in-beam studies have been performed on this nucleus using independent γ-ray and conversion electron spectroscopy [7–9]. Two different band-head configurations for the yrast bands are discussed for ^{253}No in the literature, namely the $7/2^+[624]$ and $9/2^-[734]$ (the latter forming the ground state). Data obtained from a GAMMASPHERE study favoured the $7/2^+[624]$ band-head configuration, which identified two rotational bands with the intensity flow predominantly through stretched $E2$ multipolarity intraband transitions [8]. From this previous study, the yrast bands were determined to lie 355 keV above the ground state, and linked to the ground state via a multiplet γ-ray decay. A subsequent γ-ray study using JUROGAM II at the University of Jyväskylä (JYFL) measured the interband $M1$ transitions in addition to the stretched intraband $E2$ transitions, extended the level scheme to higher spins, and assigned the $9/2^-[734]$ ground-state configuration to be the band-head.

An in-beam internal conversion electron (ICE) study using the SACRED spectrometer at JYFL also found relatively strong mixed interband transitions [9]. In nobelium

[a] *Present address*: GSI - Helmholtzzentrum für Schwerionenforschung GmbH, 64291 Darmstadt, Germany; e-mail: a.k.mistry@gsi.de
[b] *Present address*: Argonne National Laboratory, 9700, South Cass Ave, Lemont, IL 60439, USA.
[c] *Present address*: University of Jyvaskyla, Department of Physics, P.O. Box 35, FI-400 Jyvaskyla, Finland.

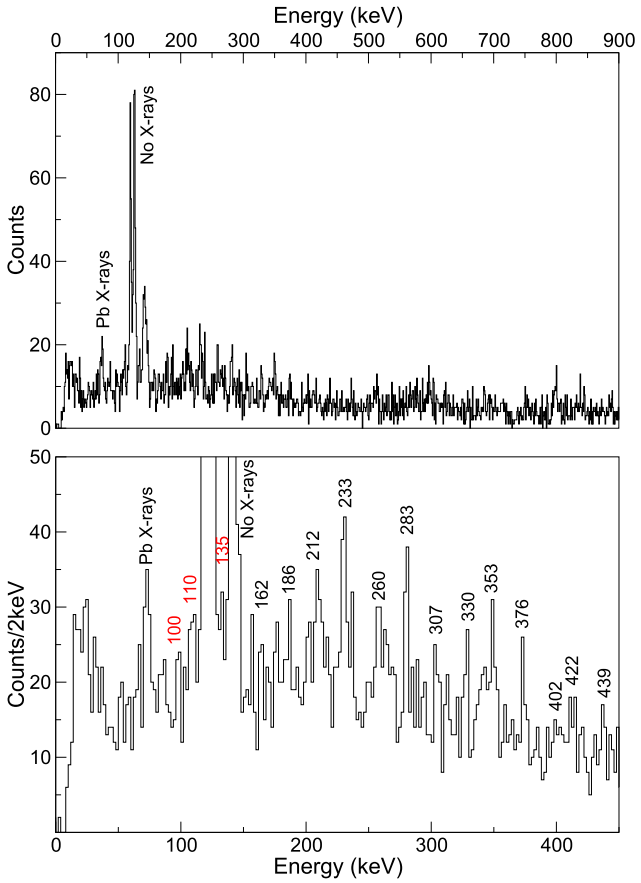

Fig. 1. Top panel: the recoil-tagged γ-rays measured by JUROGAM II. The K_α and K_β X-ray lines are the most dominant in the spectrum, resulting from the high rates of internal conversion taking place. Bottom panel: the top panel expanded to show the energy region of interest. $E2$ intraband transitions are labelled in black and interband mixed transitions in red.

nuclei, internal conversion dominates over γ-ray emission for $E2$ transition energies below 200 keV. Thus in the absence of high statistics it becomes essential to perform simultaneous conversion electron and γ-ray measurements to gain a complete picture of the structure of the nucleus. The SAGE spectrometer offers this advantage, allowing coincidences to be established for γ rays and electrons in the same measurement, thus avoiding the need for normalisation of intensities measured in two different experiments. In this study such coincidences have allowed the lower-spin region of the level scheme to be established. In addition, this study assesses the performance of SAGE with limited statistics and provides confirmation of the previously determined band-head configuration.

2 Experimental details

The experiment was performed at JYFL, Finland with the SAGE spectrometer coupled to the RITU gas-filled separator [10,11]. SAGE comprises the JUROGAM II germanium-detector array for γ-ray spectroscopy and a highly segmented silicon detector for electron detection [12]. A solenoidal magnetic field was used to transport the electrons to the silicon detector, while a high-voltage barrier reduced the flux of low-energy (< 40 keV) δ electrons produced by the interaction between beam and target particles. The absolute detection efficiencies measured shortly before the study were $8.2 \pm 0.2\%$ at 223 keV for JUROGAM II and $7.0 \pm 0.5\%$ at 155 keV for the electron spectrometer. A $^{48}Ca^{10+}$ ion beam was accelerated and incident upon a ^{207}Pb target for 215 hours with an average beam intensity of 8 pnA. The nuclide ^{253}No was produced in the reaction ^{207}Pb(^{48}Ca, 2n)^{253}No with a cross section of approximately 1 μb [13]. The Pb target had a thickness of $\sim 400\,\mu$g/cm^2 with $50\,\mu$g/cm^2 carbon layers on either side of the target. After compound nucleus formation, the emission of two neutrons, and prompt γ rays and electrons, the evaporation residues passed through the RITU gas-filled separator and were implanted into the GREAT focal-plane spectrometer [14] for decay spectroscopy measurements. The data acquisition system employed the total data readout technique, with all data being read out and time stamped to 10 ns precision [15], with the lack of a common trigger reducing the dead time. The data subsequently underwent a correlation analysis using the GRAIN software package [16]. A total of 5900 recoils correlated within three half-lives (5.1 min) prior to a ^{253}No alpha decay were identified based on the measured half-life in this study $T_{1/2} = (1.7 \pm 0.2)$ min and energy $E_\alpha = (8090 \pm 36$ keV). These are consistent with the literature values $T^{lit}_{1/2} = (1.62 \pm 0.15)$ min and $E^{lit}_\alpha = (8010 \pm 20)$ keV [17]. The recoil-tagging technique was employed [18,19] to correlate prompt electromagnetic decays at the target position with evaporation residues (ER) transported to the focal plane of the separator.

3 Results and discussion

The top panel of fig. 1 shows the γ-ray energy spectrum measured with JUROGAM II correlated with ^{253}No recoils (recoil-tagged) detected in the focal plane. Strong K_α and K_β X-ray peaks dominate the spectrum between 120 keV and 140 keV, an indication of the high degree of internal conversion occurring. In the bottom panel, the spectrum is expanded to the region of interest in this analysis. The γ-ray energy peaks that are confirmed in this study are labelled. Additional peaks that are evident probably stem from populated non-yrast side bands that could not be definitively assigned.

A similar energy spectrum is measured in fig. 1 as observed in [9], albeit in this case with lower statistics. In this previous study, the higher-energy γ-ray peaks were identified as $E2$ transitions in two yrast rotational bands, with some lower-energy transitions placed as interlinking transitions between the two bands, based on a γ-γ coincidence analysis.

The prompt electron spectrum is presented in fig. 2. The recoil-tagging technique was applied, with the condition of demanding the time difference between electron

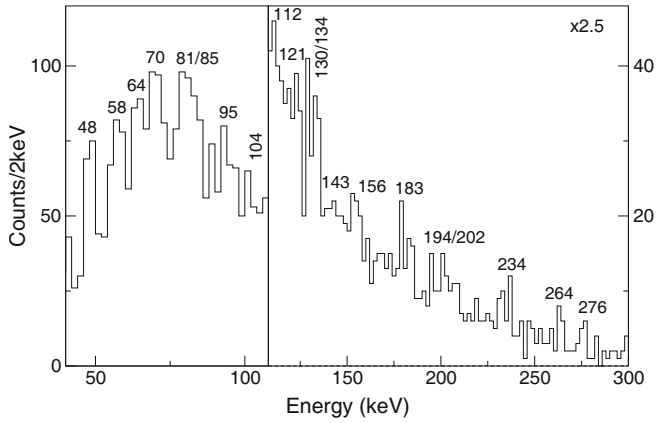

Fig. 2. Recoil-tagged electrons with an additional anticoincidence applied (see text). The electron peaks are labelled by the measured electron energy and the transition energies are given in table 1.

detection at the target position, and evaporation residue detection at the focal plane. Background was subtracted by applying an anticoincidence timing condition on the region around the recoil-electron timing peak. It is important to note that there are known side bands in ^{253}No [4,6] that can contribute additional γ-ray and electron detections, hence the observed fragmented nature of the intensity over a number of transitions. The large background at low energies in the electron spectrum is therefore made up of the residual δ electron flux and electrons emitted in the decay via unresolved bands populated in the reaction, as seen previously in the neighbouring ^{254}No isotope [20].

Given the low statistics and the resolution (FWHM) of the device during operation of 3 keV for gamma rays and 6 keV for conversion electrons, all energies obtained in this study are accurate to no better than ± 3 keV (1σ).

3.1 Statistical analysis

As the present study is performed at the limit of experimental sensitivity, special attention has to be paid to the statistical significance of any results. Two approaches were utilised: If the net peak area (counts above the average background) is at or above 10 counts then significance is assessed assuming a Gaussian distribution. Below 10 counts Poisson statistics differ sufficiently from Gaussian statistics and a limit [21] determining whether the net area of a peak is significant can be given as

$$L_c = 2.33\sqrt{B} \quad (1)$$

with a 95% confidence limit, where B is the background count underneath the peak area. For each peak assessed with this method, the region of interest was defined by an area of ± 6 keV (SAGE resolution) around the highest counting channel.

When Poisson statistics are used, then a careful consideration of the background region must be taken into account when assessing the validity of a peak. Assume that the number of counts in the region of interest in a randomly generated sample is given as x, and the mean background rate (in a region around the peak) is λ. The number of counts above the background must be significant enough to give a confidence limit of 95% to assign a peak. If one knows the number of counts in the background, a minimum number of counts above the background can be established for a given confidence limit from tabulated values on Poisson statistics. As an example if the given background count is $\lambda = 2$, then the minimum number of counts above the background, for a 95% confidence limit gives $x = 4$ counts. In this study all peaks labelled were found to be at or above the 95% confidence limit assigned for when either Gaussian or Poisson statistics were applied.

Table 1. Electron energies of peaks in the recoil-tagged prompt electron spectrum, and the K, L, M, and $N+$ shell transitions to which they correspond. Energies highlighted in **bold** are potential $E2$ intraband transitions and those in *italics* are proposed $M1 + E2'$ interband transitions. Potential overlapping contributions are highlighted in ***bold italics***. All energies are within ± 3 keV of the final assigned energy values.

e^- *energy* (keV)	K (keV)	$L_I + L_{II}$ (keV)	L_{III} (keV)	$M_{I\ldots V}$ (keV)	$N+$ (keV)
48	—	*76*	—	—	—
58	—	*87*	—	*62*	—
64	**213**	—	*86*	—	*64*
70	—	*99*	—	*78*	—
81	—	*110*	*103*	*89*	—
85	**234**	—	*107*	—	*85*
95	—	*124*	—	*103*	—
104	—	***135***	*126*	*112*	—
112	**261**	—	***134***	—	*112*
121	—	*149*	—	—	—
130	—	***160***	—	***138***	—
134	**283**	—	—	—	***134***
143	—	*172*	**165**	—	—
156	**305**	*184*	—	**164**	—
183	**332**	**212**	—	*193*	*183*
194	—	—	—	—	*194*
202	**351**	*231*	—	*210*	—
234	—	**262**	—	—	—
264	—	—	**286**	—	—
276	—	**305**	—	**284**	—

3.2 Level scheme construction

Previous in-beam studies on ^{253}No initially established the rotational yrast band structure [8] with de-excitation through stretched $E2$ transitions. Subsequent studies [7,9] confirmed these bands and saw the interlinking transitions between the two bands. The studies enabled up to spin $I^\pi = 45/2^-$ to be reached in the yrast bands. However the transitions at the lowest spins of the bands (from

Table 2. Multipolarities (MP) and transition energies assigned in this study compared with previous measurements. Uncertainties are to within ±3 keV. Statistical agreement is found in the majority of the measurements with the exception of some of the lower-lying transitions. *The energy assigned from electrons is labelled by an asterisk.*

MP	Measured	Reiter *et al.* [8]	Herzberg *et al.* [9]	Antalic *et al.* [6]
(σL)	(keV)	(keV)	(keV)	(keV)
	62*	–	(62)	64.1
	76*	–	(70)	76.0
	86	–	(86)	88.5
	100	–	98	99.0
	110	–	110	109.9
	124*	–	123.5	–
$M1 + E2'$	135*	–	135.5	–
	149*	–	147.5	–
	160*	–	160	–
	172*	–	171	–
	183*	–	181.5	–
	193*	–	195	–
	136*	–	(132)	–
	162	–	(156)	156
	186	–	(184)	–
	212	207	208	209.2
	233	234	233.5	–
	260	259	259	255.1
$E2$	283	284	283	–
	307	309	307.2	–
	330	334	331	–
	353	355	352.5	–
	376	377	376.5	–
	402	398	398	–
	422	417	421	–
	439	436	440	–

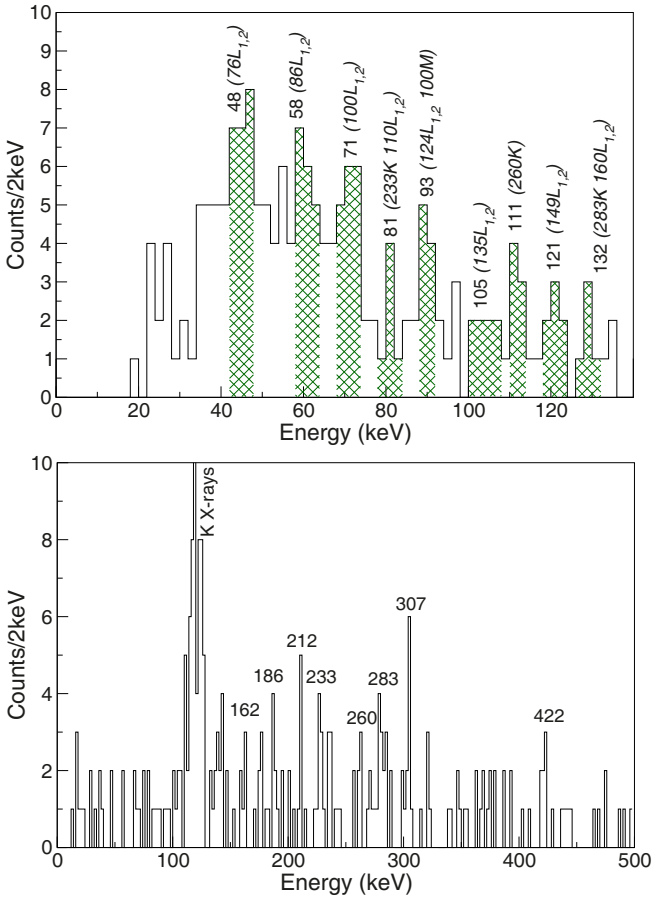

Fig. 3. Top panel: ICEs in coincidence with the $K\alpha_1$ X-rays in the γ projection of the recoil-tagged γ-e^- matrix in the region of interest. Bottom panel: gamma rays coincident with the electrons from the cross-hatched regions in the top panel. Some of the $E2$ transitions are evident and labelled.

$I^\pi = 15/2^-$ and lower spins) were only tentatively accessible, due to lower detection efficiencies at these energies. A comparison between measured transition energies from previous studies [6,8,9] and this work is given in table 2. One of the strengths of SAGE is that it is sensitive to both intra- and interband transitions, with the former most readily observed in γ rays and the latter in conversion electrons. Thus using SAGE gives greater scope in constructing a level scheme in this mass region where internal conversion can be the dominant de-excitation mechanism. Using the coincidences between γ rays and conversion electrons allows one to observe transitions throughout the band. An example of this is given in fig. 3. The top panel shows electrons in coincidence with K_α X-rays. In the bottom panel gamma rays in coincidence with electrons from the shaded regions are shown to illustrate the statistics of the study.

The level scheme proposed in fig. 4 was built using the recoil-tagged γ-ray and electron cross-coincidences, with the transition energies assigned from these values. Due to the high number of energetically similar transitions, and low statistics, coincidences set on γ rays were carefully examined to give electron spectra and vice versa. In fig. 4, transitions that were previously unassigned by in-beam studies are highlighted in red. The lower-energy transitions which were previously tentatively assigned [9] are confirmed with the aid of the electron spectrometer. Deviation in the energy assignments between the studies stem from the limited statistics in both studies. Transitions that were previously assigned but differ in this study are highlighted in the plot with asterisks. The energy values are in agreement with the focal-plane study [6] which observed the lower-energy yrast band transitions following depopulation into the yrast band structure from a side band populated by a multi-quasiparticle high-K isomer. The aforementioned study was not able to give unambiguous level scheme assignments and is in agreement with Lopez-Martens [4] that the transitions may be admixtures with similar energies across more than one band. To disentangle such a scenario would require an increased level of statistics at the focal plane to fully establish the link between the non-yrast and yrast band and the structure built on

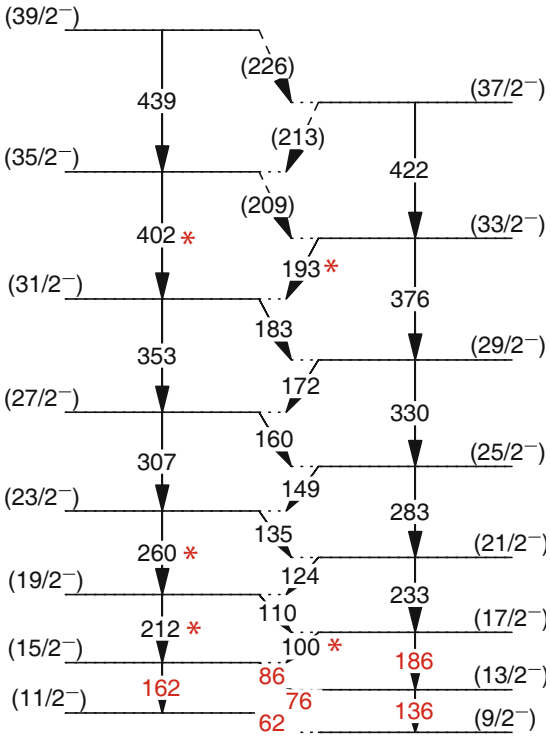

Fig. 4. Proposed level scheme based on a γ-electron coincidence analysis. Transitions in red are established through in-beam measurements in this study. The spins are tentatively assigned. Transitions with * differ in this study from those given in [9].

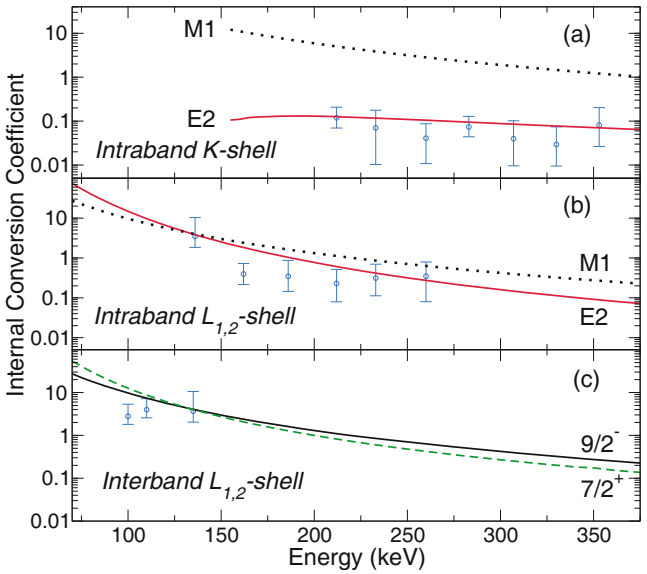

Fig. 5. ICCs plotted as a function of energy. (a) Intraband K-shell $E2$ transitions. (b) Intraband $L_{1,2}$-shell $E2$ transitions. BrIcc calculated values [22] are given by the red solid lines for pure $E2$ and black dotted lines for pure $M1$ transitions in (a) and (b). (c) Interband $L_{1,2}$-shell $M1 + E2'$ transitions compared with BrIcc values dependent upon mixing ratios for the $7/2^+[624]$ band-head (green dashed line) and $9/2^-[734]$ band-head (black solid line).

top of the non-yrast structure. The data in [4,6] suggest that the levels above the $I^\pi = 15/2^-$ state are not significantly populated by the side band structure, and thus their impact on the upper part of the level scheme in this in-beam study with spins up to $I^\pi = 39/2$ may be considered as small.

3.3 Intensity measurements

Conversion coefficient measurements are very sensitive to the multipolarity of transitions and hence become very useful for spin and parity assignments. Using the recoil-tagged γ rays and electrons, the K- and L-shell conversion coefficients were measured for most observed transitions. In some cases, electron intensities needed to be deconvolved into contributions stemming from different transitions (*e.g.*, the 64 keV electron peak is a combination of K-shell electrons from the 212 keV transition and $L_{1,2}$-shell electrons from the 86 keV transition). In such cases the contributions of electron intensity to a peak due to the overlap of K- and L-shell components was deduced from the calculated ICCs [22], with the major uncertainty stemming from the $M1/E2$ mixing ratio of the transitions. The γ rays are independent of such deconvolutions, removing any circular arguments.

The 76 keV, 86 keV and 124 keV ICC measurements are not possible given that the γ rays form doublets with the strong X-rays of lead (from the target) and nobelium. Measured ICCs are plotted in fig. 5 together with theoretical calculations using the BrIcc [22] conversion coefficients. The intraband transitions are clearly confirmed as pure $E2$ transitions within the margin of uncertainty. For the $L_{1,2}$ $M1{+}E2'$ transitions, there is a mixing between competing $M1$ and $E2$ (given here as $E2'$ for clarity) multipolarities. The calculated multipole mixing ratios for the two potential band-head configurations are taken as $\delta_{9/2^-} = 0.22$ and $\delta_{7/2^+} = 1.18$ from model calculations using the Dönau and Frauendorf method [23].

Experimentally, the multipole mixing between the competing $M1$ and $E2'$ components can be determined through the measurement of the internal conversion coefficients

$$\alpha_m = \frac{\alpha_{M1} + \delta^2 \alpha_{E2}}{1 + \delta^2}, \qquad (2)$$

where α_m is the measured ICC, and $\alpha_{M1(E2)}$ are the calculated pure, unmixed ICCs for $M1$ and $E2$ transitions. Here, a value was obtained for the mixing $\delta = 0.4^{+0.3}_{-0.1}$ as a mean value across the three measured points. The large uncertainties in the present case render such a result not precise enough to draw solid conclusions.

A key spectroscopic indicator of single-particle structure is through the determination of the $B(M1)/B(E2)$ ratio in coupled rotational bands. This factor is established from the transition intensity ratios through the bands, which is in turn dependent on the single-particle g_K-factor and hence can be used as a tool for determining the band-head configuration. The g_K-factors for the

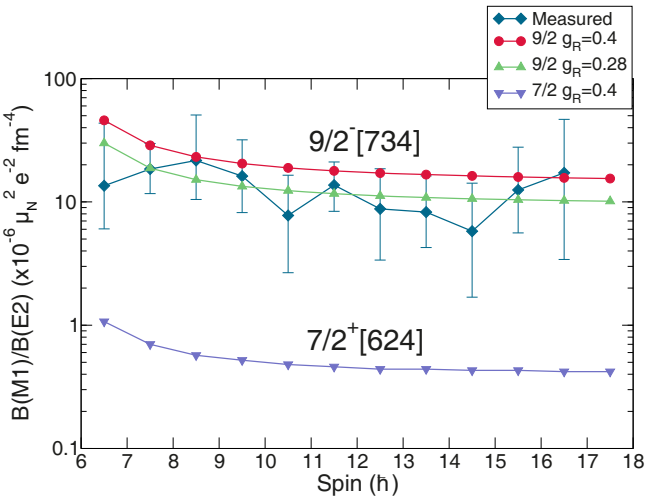

Fig. 6. The $B(M1)/B(E2)$ ratio plotted as a function of spin. The calculated values are plotted for the $9/2^-[734]$ ($g_K = -0.25$) quenched and unquenched g_R-factor, and for the $7/2^+[624]$($g_K = +0.28$). The spin given is that of the initial level the transition depopulates. For a quenched g_R for the 7/2 case, g_R=g_K and the ratio vanishes.

potential band-head configurations considered here are $g_K = -0.25(9/2^-[734])$ and $g_K = +0.28$ $(7/2^+[624])$. Values of the single-particle g_K-factors were utilised in [7] and [9] based on calculations of a deformed shell model with Wood-Saxon parametrisation. Experimentally the $B(M1)/B(E2)$ ratio can be calculated from the intensity ratio between the intraband and interband transitions

$$\frac{B(M1)}{B(E2)} = \frac{\lambda}{1.43\times10^4}\,\frac{1}{(1+\delta^2)}\,\frac{[E_\gamma(\Delta I=2)]^5}{[E_\gamma(\Delta I=1)]^3}\ (\mu_N^2 e^{-2}\,\mathrm{fm}^{-4}), \tag{3}$$

where λ is the intensity ratio ($\lambda = T(M1+E2';\ I \to I-1)/T(E2; I \to I-2)$) and δ is the multipole mixing ratio between the competing $M1$ and $E2'$ components (determined from the Dönau and Frauendorf method). The intensities for the intraband ($T(I \to I-2)$) transitions were extracted from the net counts in the measured recoil-tagged γ-ray peaks and for the interband ($T(I \to I-1)$) from the recoil-tagged electron peaks with the absolute efficiencies for the germanium array and the silicon detector respectively taken into account.

The data in fig. 6 show the experimental $B(M1)/B(E2)$ values plotted with the quenched and unquenched theoretical values for the $9/2^-[734]$ and $7/2^+[624]$ configurations. Across the rare-earth isotopes there is systematic evidence for a quenching factor to be applied to the rotational g_R-factor (see [24] for an in-depth review). Here a quenching of 0.7 is used. The branching ratios expected for the quenched ($g_R^Q = 0.7(Z/A) = 0.28$) *vs.* unquenched ($g_R = (Z/A) = 0.40$) collective rotational g-factors are used as in [9]. The values are tabulated in table 3.

Comparing the two band-head configurations shows a clear preference of the data for the $9/2^-[734]$ configuration compared with the $7/2^+[624]$ configuration.

Table 3. Measured $B(M1)/B(E2)$ values. $E(I \to I-2)$ transitions were measured from γ-rays and $E(I \to I-1)$ transitions from electrons.

I^π ($\hbar$)	$E(I \to I-2)$ (keV)	$E(I \to I-1)$ (keV)	$B(M1)/B(E2)$ $10^{-6}\mu_N^2 e^{-2}\,\mathrm{fm}^{-4}$
$(13/2^-)$	136	76	$14\ ^{+30}_{-8}$
$(15/2^-)$	162	86	$19\ ^{+11}_{-7}$
$(17/2^-)$	186	100	$22\ ^{+29}_{-11}$
$(19/2^-)$	212	110	$16\ ^{+16}_{-8}$
$(21/2^-)$	233	124	$8\ ^{+9}_{-5}$
$(23/2^-)$	260	135	$14\ ^{+7}_{-5}$
$(25/2^-)$	283	149	$9\ ^{+10}_{-5}$
$(27/2^-)$	307	160	$8\ ^{+8}_{-4}$
$(29/2^-)$	330	172	$6\ ^{+8}_{-4}$
$(31/2^-)$	353	183	$13\ ^{+16}_{-7}$
$(33/2^-)$	376	193	$17\ ^{+30}_{-14}$

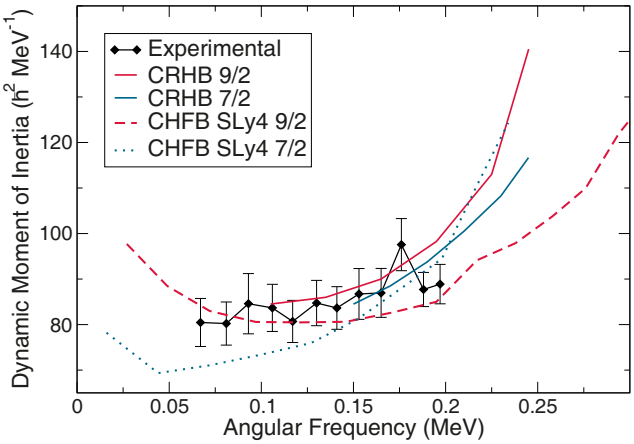

Fig. 7. The dynamic moment of inertia measured in this study. Comparisons are made between two models: cranked relativistic Hartree-Bogoliubov (CRHB) [25] and Hartree-Fock-Bogoliubov with Skyrme parametrisation [26].

It is interesting to compare the moments of inertia (MoI) calculated with the present spin assignments with those calculated by theory. If one compares the dynamic moment of inertia data to two models (cranked relativistic Hartree-Bogoliubov [25], and Hartree-Fock-Bogoliubov with Skyrme SLy4 parametrisation [26]) with experimental data from this study (fig. 7), then one can see that in the energy region probed, the data are not precise enough and both models give a good description of the nucleus. For higher spins the models predict different degrees of upbending depending on the configuration. For lower angular frequencies, the SLy4 model for the 9/2 spin shows some trend towards the data, with the CHFB SLy4 7/2 model giving lower values for MoI compared with the CHFB SLY4 9/2. In order to examine the behaviour of models with higher precision, it is necessary to attain higher spins with a greater level of statistics to reduce the statistical uncertainties.

4 Summary

Using the SAGE spectrometer, the odd-A nucleus ^{253}No was studied through combined in-beam γ-ray and electron spectroscopy. Cross-coincidences between both decay modes have enabled the confirmation of the transition energies and level ordering of the lower-spin region of the level scheme with the spin region $I^\pi = 39/2^- \rightarrow I^\pi = 9/2^-$ probed, tracing the yrast bands to the bandhead. The measured branching ratios between strongly coupled rotational bands confirm assignment of the structure being built on the $9/2^-[734]$ Nilsson configuration. Further, comparisons have been made with experimental ICCs and model calculations in this heavy-element region. The study demonstrates the performance of the SAGE spectrometer at the lower limit of production cross section for an in-beam experiment.

This work has been supported by the Academy of Finland under the Finnish Center of Excellence Programme (2012-2017). The authors also thank the GAMMAPOOL European Spectroscopy Resource for the loan of the detectors for the JUROGAM II array. Support has also been provided by the EU 7th framework programme, Project No. 262010 (ENSAR) and the UK Science and Technology Facilities Council.

References

1. R.-D. Herzberg, P.T. Greenlees, Prog. Part. Nucl. Phys. **61**, 674 (2008).
2. Ch. Theisen *et al.*, Nucl. Phys. A **944**, 333 (2015).
3. P.T. Greenlees *et al.*, Phys. Rev. Lett. **109**, 012501 (2012).
4. A. Lopez-Martens *et al.*, Nucl. Phys. A. **852**, 15 (2011).
5. F.P. Heßberger *et al.*, Eur. Phys. J. A **48**, 75 (2012).
6. S. Antalic *et al.*, Eur. Phys. J. A **47**, 62 (2011).
7. R.-D. Herzberg *et al.*, Eur. Phys. J. A **15**, 205 (2002).
8. P. Reiter *et al.*, Phys. Rev. Lett. **95**, 032501 (2005).
9. R.-D. Herzberg *et al.*, Eur. Phys. J. A **42**, 333 (2009).
10. M. Leino *et al.*, Nucl. Instrum. Methods B **99**, 653 (1995).
11. J. Sarén *et al.*, Nucl. Instrum. Methods A **654**, 508 (2011).
12. J. Pakarinen *et al.*, Eur. Phys. J. A **50**, 53 (2014).
13. Yu.Ts. Oganessian *et al.*, Phys. Rev. C **64**, 054606 (2001).
14. R.D. Page *et al.*, Nucl. Instrum. Methods A **204**, 634 (2003).
15. I. Lazarus *et al.*, Nucl. Sci. IEEE Trans. **48**, 567 (2001).
16. P. Rahkila, Nucl. Instrum. Methods A **595**, 637 (2008).
17. A.K. Jain, S. Singh, J.K. Tuli, Nucl. Data Sheets **107**, 1027 (2006).
18. K.-H. Schmidt *et al.*, Phys. Lett. B **168**, 1 (1986).
19. E.S. Paul *et al.*, Phys. Rev. C **51**, 78 (1995).
20. R.D. Humphreys *et al.*, Phys. Rev. C **69**, 064324 (2004).
21. L.A. Currie, Anal. Chem. **40**, 586 (1968).
22. T. Kibedi *et al.*, Nucl. Instrum. Methods A **589**, 202 (2008).
23. F. Dönau, Nucl. Phys. A **471**, 469 (1987).
24. N. Stone, EPJ Web of Conferences **63**, 01017 (2013).
25. A.V. Afanasjev *et al.*, Phys. Rev. C **67**, 024309 (2003).
26. M. Bender, P. Heenen, P. Reinhard, Rev. Mod. Phys. **75**, 354 (2003).